The Plant Cell, Vol. 14, 2369–2381, October 2002, www.plantcell.org © 2002 American Society of Plant Biologists

Spatiotemporal Patterning of Reactive Oxygen Production and Ca^{2+} Wave Propagation in Fucus Rhizoid Cells

Susana M. Coelho,[a,b] Alison R. Taylor,[a] Keith P. Ryan,[a] Isabel Sousa-Pinto,[c] Murray T. Brown,[b] and Colin Brownlee[a,1]

[a] Marine Biological Association of the United Kingdom, Citadel Hill, PL1 2PB Plymouth, United Kingdom
[b] Department of Biological Sciences, University of Plymouth, Drake Circus, PL4 8AA Plymouth, United Kingdom
[c] Centro Interdisciplinar de Investigação Marinha e Ambiental, Universidade do Porto, Rua do Campo Alegre, 4100 Porto, Portugal

Both Ca^{2+} and reactive oxygen species (ROS) play critical signaling roles in plant responses to biotic and abiotic stress. However, the positioning of Ca^{2+} and ROS (in particular H_2O_2) after a stress stimulus and their subcellular interactions are poorly understood. Moreover, although information can be encoded in different patterns of cellular Ca^{2+} signals, little is known about the subcellular spatiotemporal patterns of ROS production or their significance for downstream responses. Here, we show that ROS production in response to hyperosmotic stress in embryonic cells of the alga *Fucus serratus* consists of two distinct components. The first ROS component coincides closely with the origin of a Ca^{2+} wave in the peripheral cytosol at the growing cell apex, has an extracellular origin, and is necessary for the Ca^{2+} wave. Patch-clamp experiments show that a nonselective cation channel is stimulated by H_2O_2 and may underlie the initial cytosolic Ca^{2+} increase. Thus, the spatiotemporal pattern of the Ca^{2+} wave is determined by peripheral ROS production. The second, later ROS component localizes to the mitochondria and is a direct consequence of the Ca^{2+} wave. The first component, but not the second, is required for short-term adaptation to hyperosmotic stress. Our results highlight the role of ROS in the patterning of a Ca^{2+} signal in addition to its function in regulating cell wall strength in the Fucus embryo.

INTRODUCTION

Reactive oxygen species (ROS) are produced by plant and animal cells in response to a range of stimuli (Bac et al., 1997; Minibayeva et al., 1998; Tan et al., 1998; Grant and Loake, 2000). Such oxidative bursts can underlie antimicrobial activity or downstream responses such as modulation of gene expression and cell cycle control (Finkel, 1998; Reichheld et al., 1999; Bowie and O'Neill, 2000; Desikan et al., 2000; Shackelford et al., 2000). In plants and animals, the activity of a plasma membrane NADPH oxidase is implicated as an important source of ROS. Superoxide generation at the external surface of the cells is followed by a rapid dismutation to H_2O_2, which readily crosses membranes. Inhibitors of the animal NADPH oxidase, including the suicide substrate inhibitor diphenyleneiodonium (DPI), also block the elicitor-stimulated oxidative burst in plant cells (Levine et al., 1994; Desikan et al., 1996; Pugin et al., 1997), and molecular and physiological data indicate functional and mechanistic similarities between the animal and plant NADPH oxidase related–oxidative burst. Abscisic acid has been shown to increase ROS in guard cells (Pei et al., 2000), and ROS was shown to be an intermediary in the pathway leading to abscisic acid–induced antioxidant (*CAT1*) gene expression (Guan et al., 2000). In addition to plasma membrane NADPH oxidase, mitochondria, peroxisomes, and chloroplasts are potential powerful intracellular generators of ROS (Pastori and del Rio, 1997; Morel and Barouki, 1999). Plant mitochondria can produce high levels of ROS when the activity of the enzyme alternative oxidase is suppressed (Maxwell et al., 1999). Allan and Fluhr (1997) studied ROS generation using the fluorescent dye dichlorofluorescein and showed an accumulation of oxidized dye in the chloroplasts and nucleus in intact tobacco epidermal cells, which suggests the production of ROS in these compartments. However, little information is available on the subcellular spatiotemporal dynamics of ROS production in response to specific stimuli.

A close relationship between stress-induced Ca^{2+} signals and ROS production is becoming increasingly clear from studies in both plant and animal cells. Both the Ca^{2+} dependence of H_2O_2 production (Grant and Loake, 2000) and the modulation of plasma membrane Ca^{2+} channels and

[1] To whom correspondence should be addressed. E-mail cbr@mba.ac.uk; fax 01752633102.
Article, publication date, and citation information can be found at www.plantcell.org/cgi/doi/10.1105/tpc.003285.

cytosolic Ca^{2+} (Ca^{2+}_{cyt}) by H_2O_2 (Pei et al., 2000) have been demonstrated. However, essential spatiotemporal data that would allow mechanistic interpretations of the interdependence of Ca^{2+} and ROS signals is lacking.

Two-celled *Fucus serratus* embryos comprise a polarized growing rhizoid cell and a thallus cell and experience regular and dramatic natural changes in their external osmotic conditions. Hypoosmotic or hyperosmotic treatment is known to cause transient increases of Ca^{2+} that initiate in the apical rhizoid region (Taylor et al., 1996), and the spatiotemporal patterns of hypoosmotically induced Ca^{2+} signals vary with stimulus strength (Goddard et al., 2000). These Ca^{2+} signals were shown to involve both Ca^{2+} influx across the plasma membrane and the release of Ca^{2+} from intracellular stores.

We used the suitability of Fucus embryos for microinjection, patch-clamp, and cellular Ca^{2+} imaging to understand the relationship between Ca^{2+} and ROS in the stress-signaling response pathway after hyperosmotic treatment. We demonstrate a close interdependence between Ca^{2+} and ROS signals during hyperosmotic stress. We show that there are two components in the hyperosmotic stress response. An initial ROS increase, at the plasma membrane level, is initiated a few seconds after hyperosmotic treatment and is required for the generation of a Ca^{2+}_{cyt} wave. A slower, Ca^{2+}-dependent component of ROS production is localized to the mitochondria. These results also indicate a functional role, specific to the peripheral component of ROS production, in the short-term adaptive response to hyperosmotic stress.

RESULTS

Hyperosmotic Stress Elicits Rapid Production of ROS at the Rhizoid Apex

The fluorescent probe chloromethyl-2′,7′-dichlorodihydrofluorescein diacetate (CM-$DCFH_2$-DA) was used to measure intracellular ROS production by Fucus embryos. Oxidation of $DCFH_2$ by ROS yields the fluorescent DCF. Although the oxidizing agent is believed to be either OH* or H_2O_2 (Zhu et al., 1994), it is assumed that the main ROS reported is H_2O_2 (Pei et al., 2000). In cells that were loaded with CM-$DCFH_2$-DA to visualize both early cytosolic and mitochondrial ROS production (see Methods), hyperosmotic treatment (transfer from seawater to seawater plus 2 M sorbitol) induced a fast (within a few seconds) peripheral production of ROS at the rhizoid cell apex, particularly noticeable at sites of membrane–cell wall adhesions (Figure 1B; $n = 10$). After ~40 s, ROS production also was detectable in more discrete areas in subapical regions, becoming more evident after 120 s (Figure 1B). The time course of ROS production clearly showed an earlier onset in the peripheral region compared with the subapical region (Figure 1C).

Hyperosmotic Stress Elicits a Transient Ca^{2+}_{cyt} Increase and ROS Production in Discrete Intracellular Compartments

Hyperosmotic treatment induced a transient Ca^{2+}_{cyt} increase in rhizoid cells within 10 to 12 s, coincident with a reduction in cell volume (Figures 1D and 1E; $n = 10$). This Ca^{2+}_{cyt} transient reached peak average cellular levels of 483 ± 45.2 nM within 10 s of the onset of the Ca^{2+} increase before returning to resting levels during the subsequent 24 to 40 s. Confocal ratio images revealed that the hyperosmotically induced Ca^{2+} transient initiated at a discrete location in the rhizoid apex, where the plasma membrane remained attached to the cell wall during cytoplasmic shrinkage, and propagated through the cell as a unidirectional wave with an estimated velocity of 15 μm/s, reaching peak levels of at least 1 μM (Figure 1E). The apical Ca^{2+} gradient also was apparent on return to seawater (Figure 1E, a and b). Smaller excursions at resting Ca^{2+} were observed occasionally, occurring either spontaneously or in response to return to seawater after hyperosmotic treatment. In Figure 1D, these are apparent as a small decrease from 100 to 50 nM Ca^{2+}_{cyt} at the beginning of the trace and small transient increases after the return to seawater. These small changes in resting Ca^{2+} probably were related to growth or turgor regulation (Taylor et al., 1996).

Hyperosmotic treatment also elicited an increase in ROS production in discrete intracellular compartments, as monitored by DCF fluorescence in cells preincubated for 20 min in CM-$DCFH_2$-DA and washed subsequently for 20 min. ROS started to increase within 120 s after hyperosmotic treatment (Figures 1F and 1G; $n = 25$), followed by a more rapid production after 800 s, and reached a plateau after ~20 min. Although the time to onset of this component of intracellular ROS production varied from 40 to 120 s, this always occurred after the peak (i.e., downstream) of the hyperosmotically induced Ca^{2+} increase and the fast peripheral ROS production. By direct microinjection of CM-$DCFH_2$-DA into cells, we were able to estimate the average cellular production of ROS during hyperosmotic treatment to be equivalent to ~0.05 mmol of H_2O_2 per liter of cell volume per minute.

Localization of the Oxidative Burst

Embryos that were colabeled with the fluorescent mitochondrial probe MitoTracker Red and CM-$DCFH_2$-DA showed a clear localization of ROS production to mitochondria but not to chloroplasts (Figure 2A; $n = 7$). Transmission electron microscopy and confocal fluorescence imaging of identical sections labeled with MitoTracker Red confirmed, within the limits of resolution, the mitochondrial localization of the MitoTracker dye (Figure 2B). Although the mitochondria were not all labeled equally with MitoTracker dye, fluorescence was not found in any other cell compartments. Dissipation

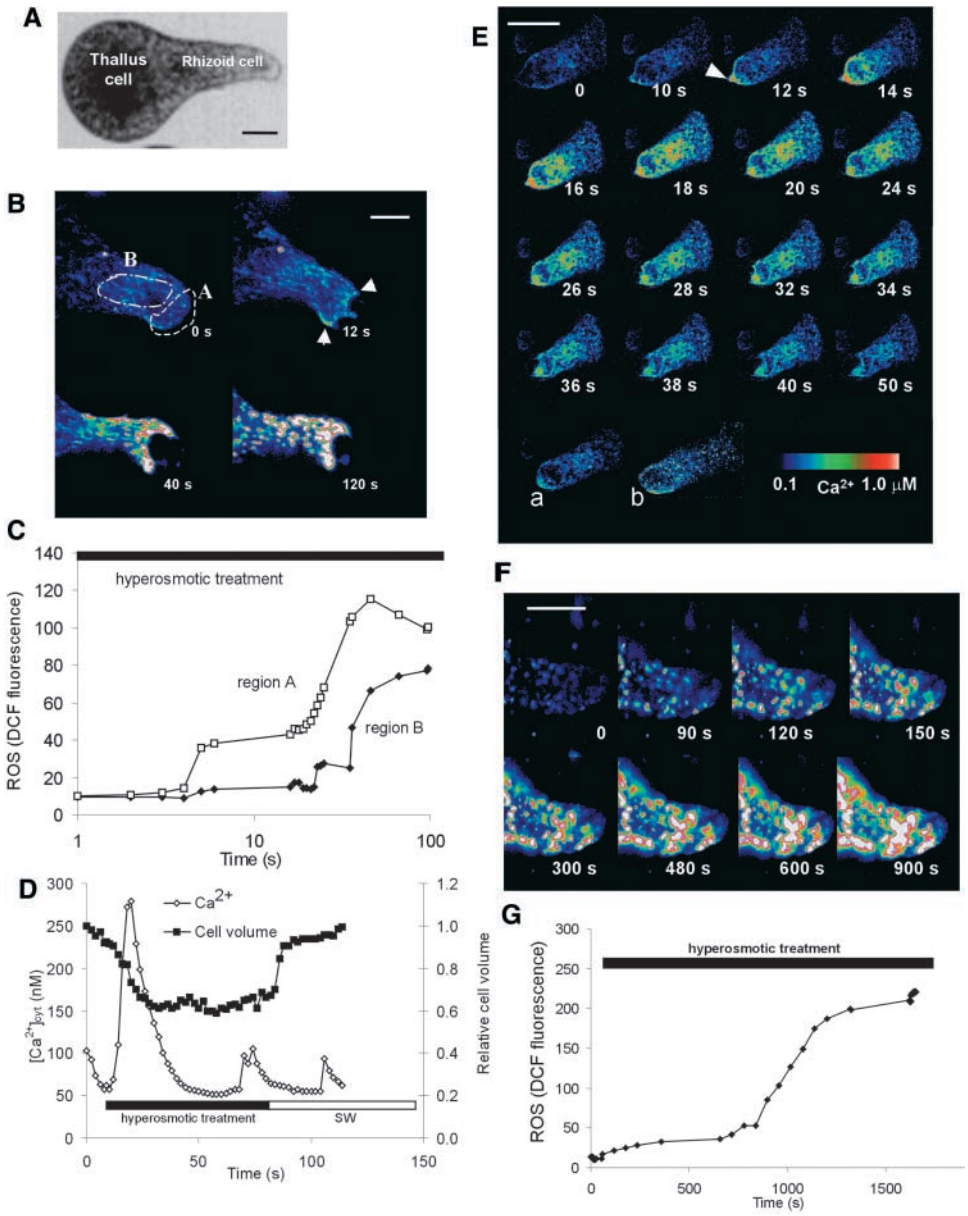

Figure 1. Time Course of Intracellular ROS Production and Ca^{2+}_{cyt} Dynamics during Hyperosmotic Treatment (Transfer from Seawater to Seawater Plus 2 M Sorbitol) in a Fucus Embryo Rhizoid Cell.

(A) Bright-field image of a two-celled Fucus embryo showing rhizoid and thallus cells. Bar = 30 μm.

(B) Early peripheral ROS production at the rhizoid apex during hyperosmotic shock. ROS production initiates at plasma membrane–wall adhesion sites (arrowheads). Cells were incubated for 20 min in 100 μM CM-$DCFH_2$-DA, immediately followed by hyperosmotic treatment. A and B represent apical and subapical regions from which mean fluorescence was plotted in **(C)**. Bar = 20 μm.

(C) Time course of DCF fluorescence in apical and subapical regions after hyperosmotic shock in the cell shown in **(B)** showing clear temporal separation of the onset of ROS production in each region.

(D) Time course of average Ca^{2+}_{cyt} increase during hyperosmotic treatment. Cell volume was computed simultaneously from transmitted light images.

(E) Confocal ratio images of a Ca^{2+}_{cyt} wave in response to hyperosmotic treatment. Ca^{2+}_{cyt} increase initiates from a point at which the plasma membrane remains attached to the cell wall (arrowhead). Localized Ca^{2+} increase at the extreme rhizoid apex was observed at 1 min (a) and 60 min (b) after return to seawater. Bar = 30 μm.

(F) Discrete localized intracellular ROS production during perfusion with hyperosmotic solution. Cells were incubated for 20 min in 100 μM CM-$DCFH_2$-DA, followed by washing in seawater for 20 min before hyperosmotic treatment. Bar = 20 μm.

(G) Time course of average cellular ROS production during hyperosmotic treatment.

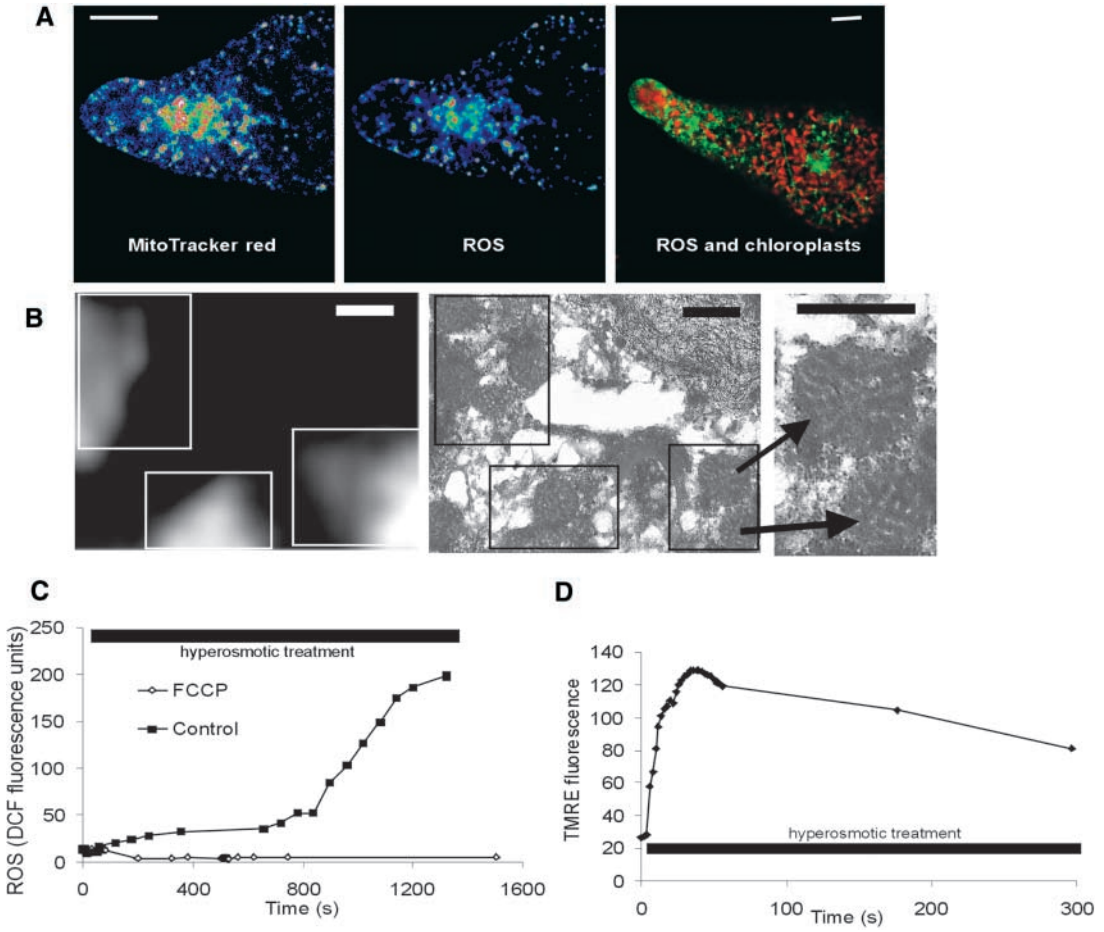

Figure 2. Mitochondrial ROS Increase.

(A) Colocalization of MitoTracker Red (left) and ROS production (center). Cells were coloaded with MitoTracker Red and CM-DCFH$_2$-DA. At right, a separate localization of chloroplasts (chlorophyll autofluorescence; red) and ROS production (green) is shown. Bar = 20 μm.
(B) Colocalization of MitoTracker Red fluorescence (left) and mitochondria (transmission electron microscopy; right) in identical fixed sections. The mitochondrial cristae are clearly visible in the enlarged transmission electron microscopy view (right). Bars = 1 μm.
(C) Carbonylcyanide *p*-trifluoromethoxyphenyl hydrazone (FCCP; 1 μM; 1 h of preincubation) caused a complete inhibition of ROS production.
(D) Hyperosmotic shock–induced depolarization of the mitochondrial membrane potential monitored as increased cellular TMRE fluorescence.

of the mitochondrial proton motive force with 1 μM carbonylcyanide *p*-trifluoromethoxyphenyl hydrazone completely abolished the hyperosmotic shock–induced mitochondrial ROS production (Figure 2C; $n = 5$). This inhibition was reversible (data not shown), suggesting a specific mitochondrial uncoupling effect.

The pattern of tetramethyl rhodamine ester (TMRE) accumulation also was identical to that of MitoTracker Green and CM-DCFH$_2$-DA (data not shown). Monitoring of the fluorescence of TMRE as an indicator of mitochondrial membrane potential suggested the occurrence of mitochondrial depolarization during hyperosmotic shock (Figure 2D; $n = 4$), the time course of which was similar to that of the corresponding transient Ca^{2+}_{cyt} increase. The mitochondrial Ca^{2+} (Ca^{2+}_{m}) reporter dye X-rhod-FF colocalized with MitoTracker Green in dual-labeling experiments (Figure 3A), allowing changes in Ca^{2+}_{m} to be monitored. An increase in Ca^{2+}_{m} was apparent ~20 s after hyperosmotic treatment (Figures 3A and 3B; $n = 15$)—that is, soon after the peak of the Ca^{2+}_{cyt} transient.

Interdependence of Ca^{2+} and ROS Production

To determine whether Ca^{2+}_{cyt} increase is essential for mitochondrial ROS production, the Ca^{2+} chelator dibromo gly-

cine, N_1N^1-(1,2-ethanediylbis(oxy-2,1-phenylene)) bis(N-carboxymethyl))-tetrapotassium salt (Br_2BAPTA) was injected into the rhizoid cell. Br_2BAPTA has been shown to prevent osmotically induced Ca^{2+} signals in Fucus rhizoids (Taylor et al., 1996). Br_2BAPTA abolished hyperosmotically induced ROS production in the injected rhizoid cell but not in the adjacent non-Br_2BAPTA-injected thallus cell (Figure 4A; $n = 7$). Thus, Ca^{2+}_{cyt} increase is a necessary step for mitochondrial ROS production.

The time course of early peripheral ROS production at the rhizoid apex was similar to that of the onset of Ca^{2+}_{cyt} increase, being detectable within a few seconds of hyperosmotic treatment. Unlike mitochondrial ROS increase, early peripheral ROS increase was not inhibited in Br_2BAPTA-injected cells (Figure 4B; $n = 12$), indicating that it occurred independently or upstream of the Ca^{2+}_{cyt} wave. The phospholipase C inhibitor U73122 blocked the hyperosmotically induced Ca^{2+} wave (Figure 4E) and the mitochondrial ROS increase but did not block peripheral ROS production (Figure 4C; $n = 7$). Interestingly, a prolonged increase of ROS was observed in the rhizoid apex in the presence of U73122 (Figure 4C). This contrasts with the more transient increase of ROS in the rhizoid apex in Br_2BAPTA-buffered cells and may reflect the inability of U73122 to block the highly localized plasma membrane influx component of Ca^{2+} increase, leading to an increase of ROS in mitochondria near the cell apex. The inactive analog of U73122 (U73343) had no effect on ROS production (data not shown).

We then investigated whether ROS production could lead to Ca^{2+}_{cyt} increase. The NADPH oxidase and peroxidase inhibitor DPI (Pugin et al., 1997; Frahry and Schopfer, 1998; Pei et al., 2000) brought about a complete inhibition of both peripheral and mitochondrial ROS increase and abolished the Ca^{2+}_{cyt} wave (Figures 4D and 4E; $n = 8$). This raises the likelihood that the peripheral ROS increase resulted from the extracellular production of ROS by the activity of plasma membrane–associated NADPH oxidase, leading to diffusion of H_2O_2 into the cell. The critical role of extracellular ROS production in initiating this cascade is further strongly supported by the dramatic inhibition of both intracellular ROS production ($n = 20$) and the Ca^{2+} wave ($n = 8$) by the application of extracellular catalase (Figures 4D and 4E). External application of H_2O_2 produced a dose-dependent increase of Ca^{2+}_{cyt} (Figures 5A and 5B; $n = 4$ for each concentration), reaching Ca^{2+}_{cyt} peak levels of 600 ± 102 nM with 1 mM H_2O_2. However, in clear contrast to the hyperosmotically induced Ca^{2+}_{cyt} transient, this did not propagate as a wave, occurring instead as a global Ca^{2+}_{cyt} increase spreading inward from around the cell periphery.

Single-channel recordings from cell-attached membrane patches of laser-derived spheroplasts from the rhizoid apex (Figure 5C) consistently revealed the presence of cation-permeable channels with properties identical to those characterized previously as nonselective cation channels (Taylor et al., 1996), based on their conductance (28 pS), reversal potential (−25 mV; assuming E_K of −50 mV, $[K^+]_{cyt} = 200$ mM) (Taylor et al., 1996), and spheroplast resting membrane potential of −60 mV (Berger and Brownlee, 1995). In 16 of 22 patches containing this type of channel activity, bath perfusion with 1 mM H_2O_2 in seawater produced a significant increase in channel activity. Although the extent of channel activation varied from cell to cell, in the experiment shown in Figure 5C, open probability averaged 0.01 before H_2O_2 addition and increased to 0.51 during the initial 10 s after H_2O_2 perfusion. Although opening to only a single open current

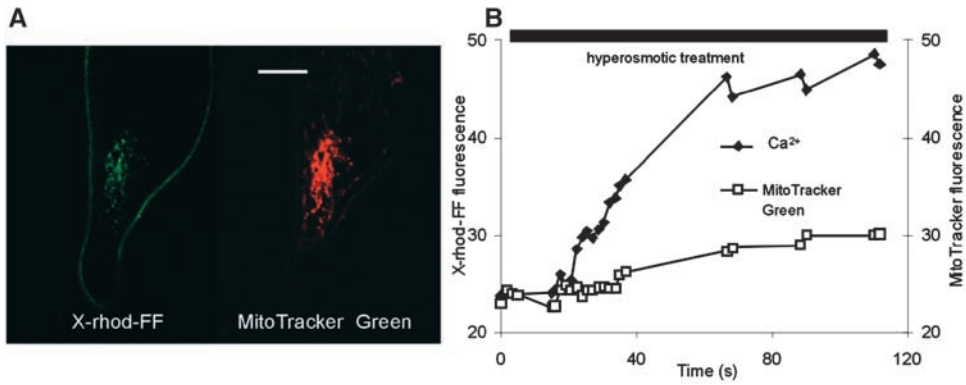

Figure 3. Ca^{2+}_m Dynamics during Hyperosmotic Treatment.

(A) Colocalization of X-rhod-FF and MitoTracker Green in mitochondria. Bar = 30 μm.

(B) Ca^{2+}_m increase during hyperosmotic treatment (black bar at top) measured with X-rhod-FF. Dual labeling with MitoTracker Green allowed Ca^{2+}-independent fluorescence to be monitored. Average X-rhod-FF or MitoTracker Green fluorescence values were plotted from the perinuclear mitochondria-rich region.

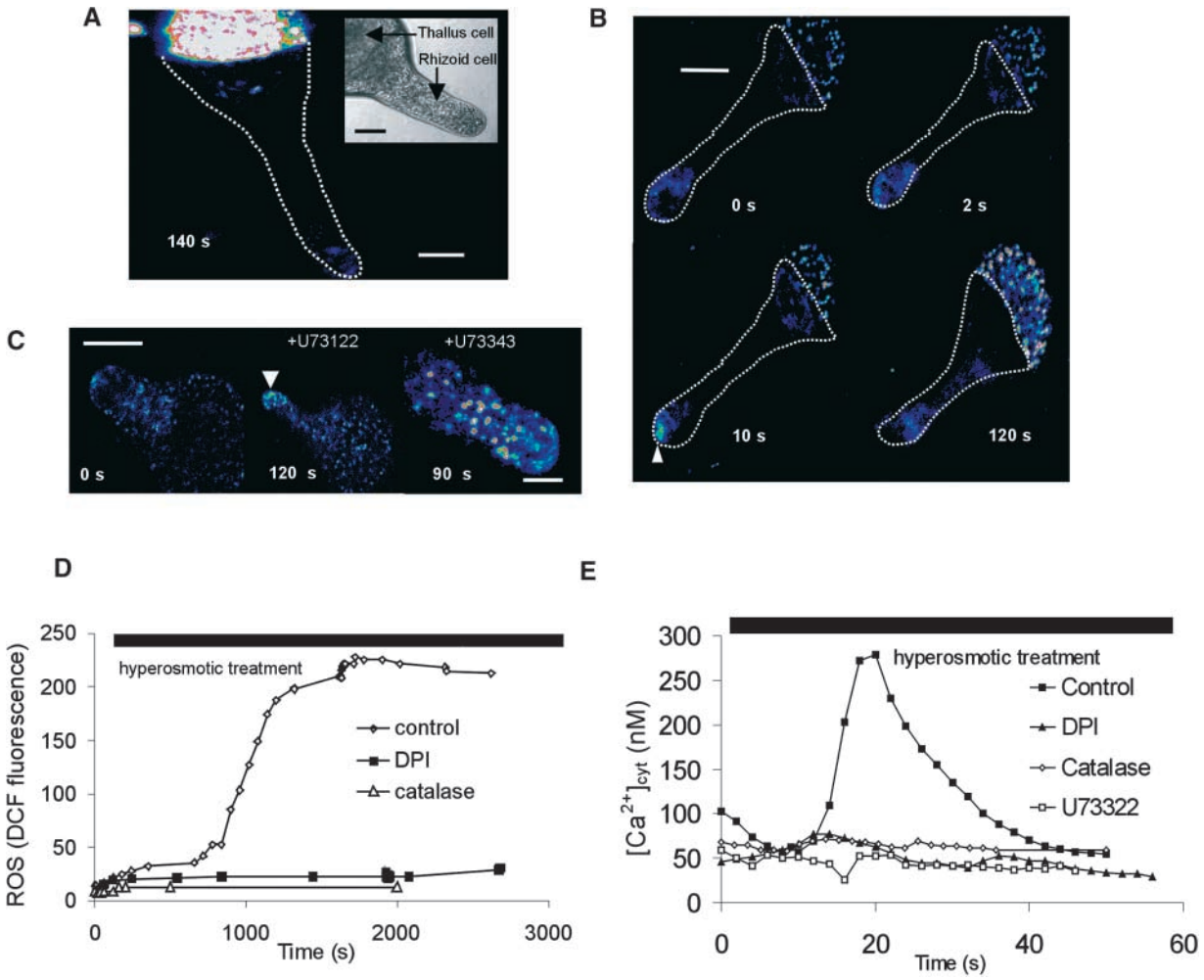

Figure 4. Interdependence between Ca^{2+}_{cyt} and ROS Production.

(A) Injection of Br_2BAPTA (4 mM final intracellular concentration) into the rhizoid cell inhibited mitochondrial ROS production (monitored at 140 s after hyperosmotic treatment) in cells loaded for 20 min with CM-$DCFH_2$-DA but not in the adjacent noninjected thallus cell. The dotted line indicates the rhizoid cell. Bar = 30 μm.

(B) Br_2BAPTA injection into the rhizoid cell did not prevent early peripheral hyperosmotically induced ROS production (arrowhead). In the cell shown, ROS production was apparent at the rhizoid apex at 2 and 10 s but declined to pretreatment levels after 120 s. Bar = 40 μm.

(C) The phospholipase C inhibitor U73122 inhibited mitochondrial but not peripheral hyperosmotically induced ROS production (left and middle). Cells were preincubated with U73122 for 2 h, and the inhibitor was retained in the hyperosmotic solution. The inactive analog U73343 did not prevent mitochondrial ROS increase. Bar = 30 μm.

(D) DPI and externally applied catalase completely inhibited ROS production during hyperosmotic shock. Cells were preincubated for 1 h in 10 μM DPI and for 30 min in 450 μg/mL catalase, and the inhibitors were retained in the perfusing hyperosmotic solution. The black bar at top indicates hyperosmotic perfusion.

(E) DPI, catalase, and U73122 abolished the hyperosmotically induced Ca^{2+}_{cyt} increase in rhizoid cells. Calcium green/Texas red ratio values were averaged for the whole rhizoid cell. The black bar at top indicates hyperosmotic perfusion.

level was observed before H_2O_2 treatment, four open levels were apparent from the single-channel trace and the associated amplitude histogram after H_2O_2 treatment (Figure 5C). The effect of H_2O_2 was variable but transient, lasting between 10 and 30 s.

Ca^{2+}_{cyt} Increase Is Sufficient to Induce Mitochondrial ROS Production

To determine whether Ca^{2+} increase alone was sufficient for mitochondrial ROS production, we used caged inositol

1,4,5-triphosphate [Ins(1,4,5)P_3] to increase Ca^{2+}_{cyt} in the absence of any stimulus. Photorelease of Ins(1,4,5)P_3 caused an immediate increase of Ca^{2+}_{cyt} (Figure 6A) that lasted for up to 20 s ($n = 6$). This Ca^{2+}_{cyt} increase was sufficient to trigger mitochondrial ROS production in the absence of any other stimulus (Figure 6B; $n = 6$). Significantly, the Ins(1,4,5)P_3-induced mitochondrial ROS production was not inhibited by DPI (Figure 6C; $n = 3$), indicating that the total inhibitory effect of DPI on hyperosmotically induced ROS production and the Ca^{2+}_{cyt} wave resulted from the specific inhibition of an upstream DPI-sensitive process.

Peripheral ROS Production Is Involved in Osmotic Adaptation

A functional role for ROS in the response to abiotic stress was evident from experiments that monitored the adaptation

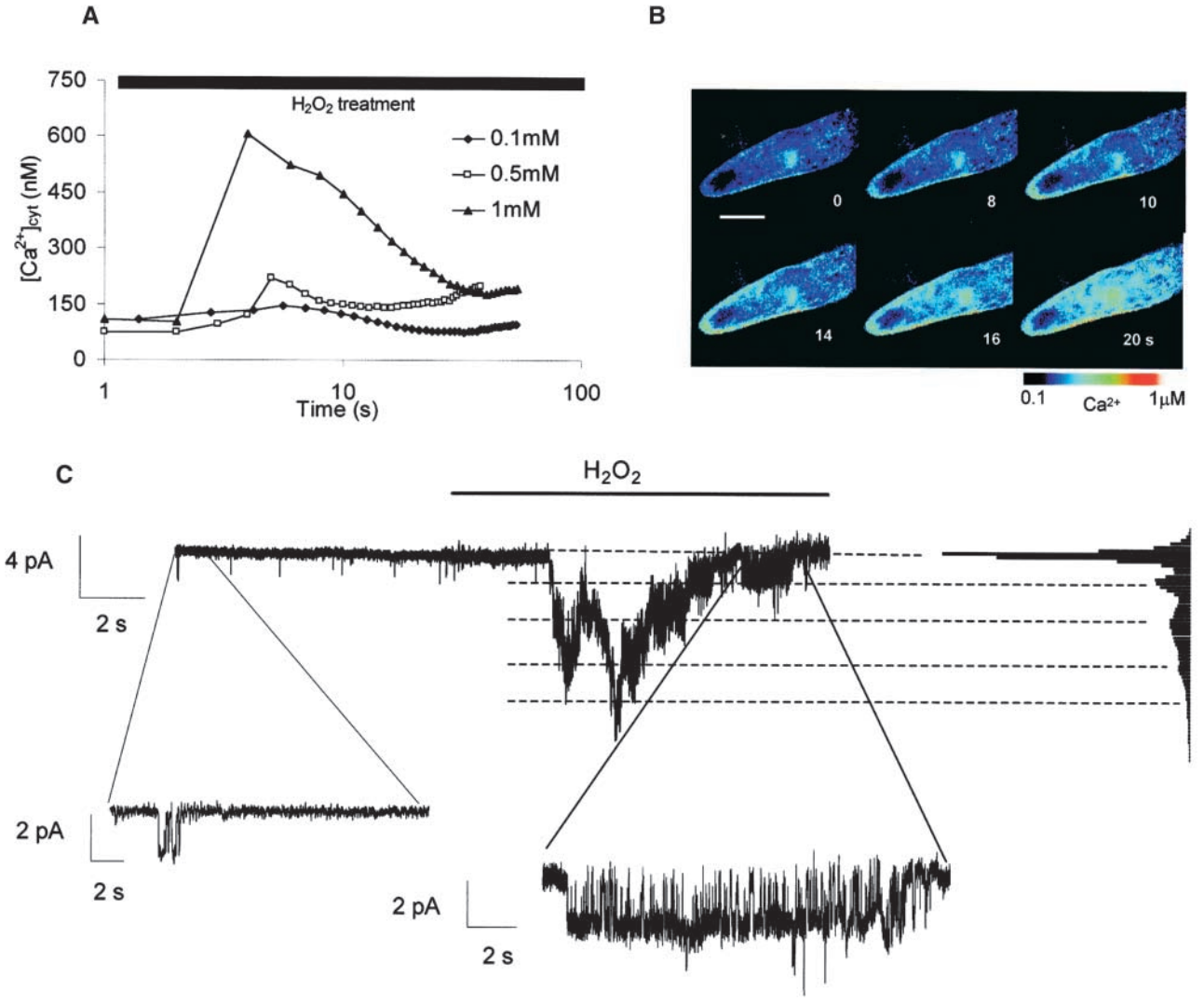

Figure 5. Changes in Ca^{2+}_{cyt} and Channel Activity Induced by Extracellular H_2O_2.

(A) Externally applied H_2O_2 caused a transient dose-dependent increase in Ca^{2+}_{cyt} in rhizoid cells.
(B) Confocal ratio images of a Ca^{2+}_{cyt} increase in response to externally applied 1 mM H_2O_2. Bar = 30 μm.
(C) Single channels recorded from a cell-attached membrane patch of a laser-derived spheroplast from the rhizoid apex. Before perfusion with H_2O_2, the patch showed single inward channel currents opening with low probability to a single level. A transient increase in channel activity was apparent within 4 s of 1 mM H_2O_2 perfusion. Four open levels induced by H_2O_2 are apparent in the channel trace and the accompanying amplitude histogram (right).

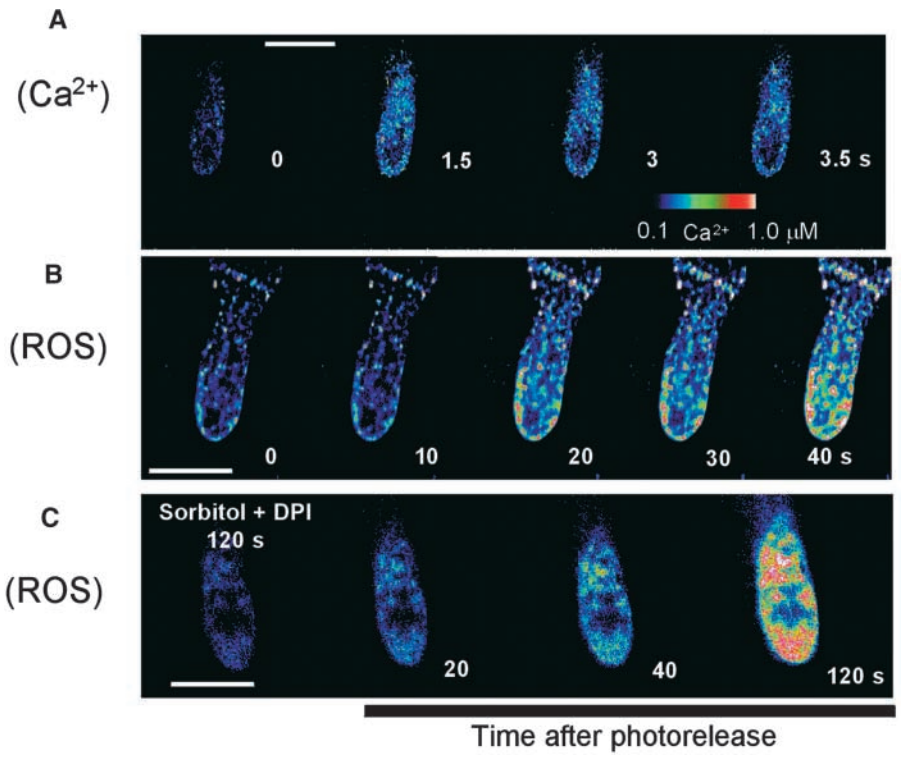

Figure 6. Ca^{2+}_{cyt} Increase Is Sufficient to Induce Mitochondrial ROS Production.

The left image in each sequence shows Ca^{2+} or ROS before photorelease of caged $Ins(1,4,5)P_3$. Images after $Ins(1,4,5)P_3$ release are identified by the bar at bottom.

(A) Ca^{2+}_{cyt} increase in response to photorelease of $Ins(1,4,5)P_3$ (1-s UV light flash given at time 0). Bar = 50 μm.

(B) ROS production induced by Ca^{2+}_{cyt} increase in response to photorelease of $Ins(1,4,5)P_3$. Bar = 40 μm.

(C) DPI prevented the hyperosmotically induced (sorbitol plus seawater) but not the subsequent $Ins(1,4,5)P_3/Ca^{2+}$-induced mitochondrial ROS production. Bar = 40 μm.

to osmotic treatments. Hypoosmotic shock (from 100% to 50% seawater) caused a significant proportion (25%) of rhizoid cells to rupture. However, hyperosmotic pretreatment rendered embryos more tolerant to osmotic bursting in response to subsequent hypoosmotic shock (Table 1), indicating increased cell wall strength. Pretreatment of embryos with 100 or 500 μM H_2O_2 also induced increases in resistance to subsequent hypoosmotic shock, suggesting that the osmotic adaptation induced by hyperosmotic pretreatment is related to ROS production. This was further supported by the complete abolition of this osmotic adaptation by DPI. By contrast, treatment of the embryos with the phospholipase C inhibitor U73122 (which blocks the hyperosmotically induced Ca^{2+} increase [Figure 4] and subsequent mitochondrial ROS production but not peripheral ROS production) did not affect the development of osmotic resistance, indicating that early peripheral ROS production is sufficient to activate cell wall resistance mechanisms.

DISCUSSION

Our results show a clear and essential interaction between Ca^{2+} and ROS in short-term signaling in response to hyperosmotic treatment. The velocity of propagation of the hyperosmotically induced Ca^{2+} wave reported here (~15 μm/s) was similar to that reported previously for hypoosmotically induced Ca^{2+} signals in Fucus rhizoid cells (Goddard et al., 2000). However, the pattern of propagation is different from that reported for hypoosmotic treatments, which generate separate apical Ca^{2+} increases and/or bidirectionally propagating Ca^{2+} waves that initiate in the perinuclear region depending on the strength of the stimulus (Goddard et al., 2000). Thus, the hyperosmotic Ca^{2+} wave provided a consistent signal against which to compare the patterns of ROS production in this signaling pathway. The hyperosmotically induced Ca^{2+} wave and the early peripheral ROS production both localize to the rhizoid apex at sites of adhesions be-

tween the plasma membrane and the cell wall. However, although the Ca^{2+} wave was dependent on the extracellular production of ROS, as indicated by the complete inhibition of the Ca^{2+} wave by both DPI and the extracellular application of catalase, early peripheral ROS production was independent of the Ca^{2+}_{cyt} increase.

A role for ROS in the spatial patterning of the Ca^{2+} wave also was indicated by the delocalized increase of Ca^{2+}_{cyt} initiating from around the cell periphery in response to delocalized external H_2O_2 application. In addition, the rapid activation by H_2O_2 of nonselective plasma membrane cation channels in cell-attached recordings strongly suggests that the initial action of external ROS production is mediated via Ca^{2+} influx through these channels. It remains to be determined whether the production of ROS at the growing rhizoid apex also underlies the Ca^{2+} gradient associated with rhizoid germination and growth (Brownlee and Wood, 1986; Taylor et al., 1996; Pu and Robinson, 1998). The concentrations of H_2O_2 that elicited increases in Ca^{2+}_{cyt} (0.1 to 1.0 mM) are comparable to those shown to cause Ca^{2+} increases and increased Ca^{2+} current in stomatal guard cell protoplasts (Pei et al., 2000). The actual H_2O_2 concentrations at the plasma membrane during hyperosmotic treatments are not known. Although we have estimated an average cellular H_2O_2 production rate of 50 $\mu mol \cdot L^{-1} \cdot min^{-1}$, the H_2O_2 concentrations at localized sites of production are likely to be considerably higher than the micromolar range.

The mitochondrial membrane potential drives ATP synthesis and provides a large driving force for divalent cation entry. Several studies have shown that, when challenged with high Ca^{2+}_{cyt}, the mitochondria can contribute to Ca^{2+} homeostasis by providing an intracellular sink for Ca^{2+} (Rizzuto et al., 2000). The increase in cellular TMRE fluorescence in response to hyperosmotic shock is consistent with the release of TMRE from the mitochondria in response to mitochondrial depolarization, resulting in reduced dye quenching (Zimmermann, 2000). We used X-rhod-FF as an indicator of Ca^{2+}_{m}. This is an improved version of rhod-2, which has been used to monitor Ca^{2+}_{m} in both animal and plant cells (Subbaiah et al., 1998; Park et al., 2001). Its colocalization with MitoTracker in the present study confirmed its mitochondrial localization in Fucus rhizoid cells. The onset of Ca^{2+}_{m} increase, coincident with the peak of the Ca^{2+}_{cyt} transient (i.e., 20 s after the hyperosmotic treatment), suggests the occurrence of Ca^{2+} uptake by the mitochondria after cytoplasmic Ca^{2+} increase, consistent with the role for mitochondria in buffering Ca^{2+}_{cyt} shown in a variety of animal cell types (Duchen, 2000; Rizzuto et al., 2000; Zimmermann, 2000). Moreover, recent reports show that the uptake of Ca^{2+} by mitochondria has a powerful impact on cellular Ca^{2+} signaling (Duchen, 2000), affecting the generation and propagation of $Ins(1,4,5)P_3$-triggered Ca^{2+} waves (Zimmermann, 2000) and the modulation of store-operated Ca^{2+} currents (Hoth et al., 1997).

To date, evidence for the role of mitochondria in spatiotemporal Ca^{2+} signaling is largely lacking for plants and algae, although mitochondria have been shown to represent a source of Ca^{2+} for signals elicited in response to anoxia (Subbaiah et al., 1998). We also show here that the onset of the increase in mitochondrial ROS production is coincident with the declining phase of the transient Ca^{2+}_{cyt} increase, with the peak of the mitochondrial depolarization, and with the increase of Ca^{2+}_{m} after hyperosmotic treatment. Moreover, mitochondrial ROS production shows an absolute dependence on Ca^{2+}_{cyt} increase. In animal cells, mitochondria may incur Ca^{2+}-induced respiratory impairment in response to Ca^{2+} loading that may potentiate ROS production (Grijalba et al., 1999). The total abolition of mitochondrial ROS production in Br_2BAPTA-injected rhizoid cells indicates a strong causal link between Ca^{2+}_{cyt} increase, Ca^{2+}_{m} uptake, and ROS production. Thus, an increase of Ca^{2+}_{cyt} is necessary to induce mitochondrial ROS production and is preceded by a peripheral cytosolic increase of ROS, involving an initial extracellular production of ROS, probably through a NADPH oxidase–like activity.

The hyperosmotically induced mitochondrial ROS production and Ca^{2+}_{cyt} increase were sensitive to DPI. By contrast, Ca^{2+}-induced mitochondrial ROS production after photorelease of caged $Ins(1,4,5)P_3$ was DPI insensitive. Therefore, hyperosmotically induced mitochondrial ROS production appears to require the activity of an upstream DPI-sensitive process.

A functional role for ROS in the response to abiotic stress was evident from experiments that monitored adaptation to

Table 1. Resistance to Hyperosmotic Shock in Pretreated and Control Embryos

Pretreatment[a]	Rhizoid Cell Bursting in Response to Subsequent Hypoosmotic Shock (% of Control)[b]
Control (no pretreatment)	100
2 M Sorbitol[c]	13.5
2 M Sorbitol + U73122	19.2
Sorbitol + DPI	101.9
100 μM H_2O_2[d]	30.8
100 μM H_2O_2 + U73122[d]	36.5
500 μM H_2O_2	23.1
500 μM H_2O_2 + U73122	23.1

[a] Pretreatments were given 1 h before a hypoosmotic shock (50% seawater).

[b] A minimum of 100 embryos were counted per replicate. Bursting was recorded at 5 min after hypoosmotic shock. Values represent the average of three replicates and are representative of two independent experiments.

[c] Sorbitol pretreatment was given for 30 min.

[d] H_2O_2 and U73122 were applied for 2 min (pretreatment with U73122 for 2 h).

osmotic treatments. Thus, hyperosmotic or H_2O_2 pretreatments rendered embryos more tolerant to osmotic bursting in response to subsequent hypoosmotic shock (Table 1). This is consistent with the widely reported role for ROS in increasing cross-linking of cell wall polymers, leading to increased cell wall strength in response to stress (Bradley et al., 1992; Fry et al., 2000). This was abolished by DPI but not by the inhibitor U73122, which blocks the Ca^{2+}_{cyt} increase and subsequent mitochondrial ROS production (Figures 4C and 4E), indicating that the early peripheral oxidative burst is sufficient to activate cell wall resistance mechanisms. The activation of cell wall resistance mechanisms by hyperosmotic treatment may function to counter the hypoosmotic stress that is likely during rehydration on return to normal seawater after solute accumulation associated with hyperosmotic adaptation.

Our results indicate a sequence of events leading to mitochondrial ROS production that involves an initial localized extracellular production of ROS at the level of the plasma membrane leading to Ca^{2+}_{cyt} increase, Ca^{2+} uptake by mitochondria, and mitochondrial ROS production (Figure 7). This is consistent with the demonstration of ROS production in response to abscisic acid in Arabidopsis stomatal guard cells, which was shown to increase the activity of hyperpolarization-dependent Ca^{2+} channels in the plasma membrane, leading to Ca^{2+}_{cyt} increase (Pei et al., 2000). The rapid onset of peripheral ROS production and Ca^{2+} increase reported here indicates a direct and rapid modulation by ROS of the pathways leading to propagation of a Ca^{2+}_{cyt} wave, involving both Ca^{2+} influx channels and release of Ca^{2+} from intracellular stores in endoplasmic reticulum–rich cellular regions in Fucus rhizoid cells (Taylor et al., 1996; Goddard et al., 2000).

These findings provide an insight into ROS/Ca^{2+} signaling in showing that localized extracellular ROS production is required for the spatial patterning of a Ca^{2+} signal. Good evidence exists for differing roles of spatially distinct Ca^{2+} signals in Fucus (Goddard et al., 2000). Although additional work is needed to establish the significance of mitochondrial ROS production in this system, peripheral ROS at the cell apex is involved in both Ca^{2+} wave generation and direct adaptive responses to stress.

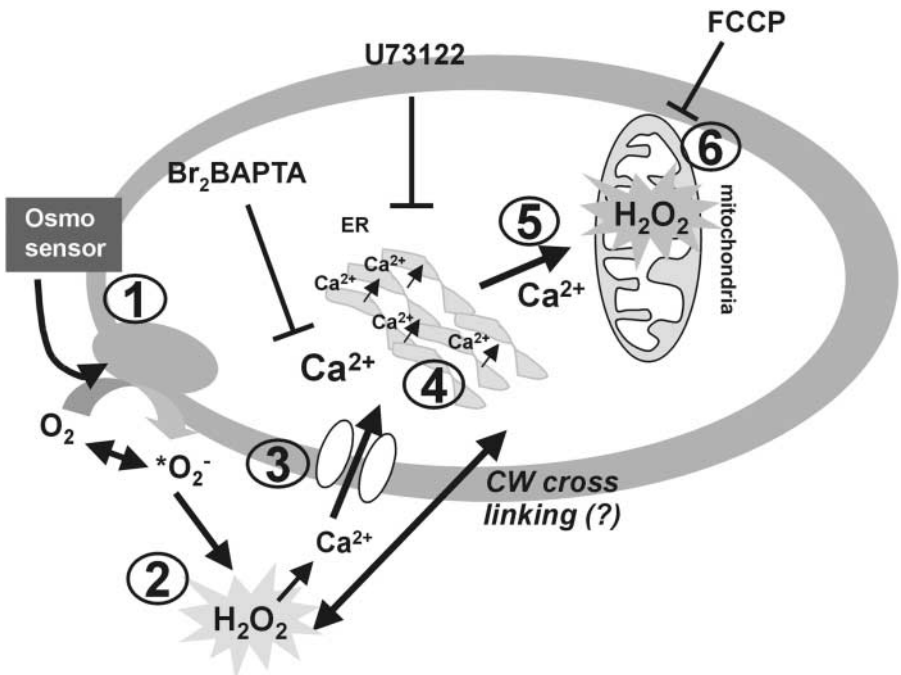

Figure 7. Proposed Signaling Pathway during Hyperosmotic Stress in Fucus Embryos.

Osmotic change is sensed by an unidentified osmosensor (1), which induces DPI-sensitive ROS production within 10 s (2). H_2O_2 is produced at the exterior side of the plasma membrane and may be involved in cell wall strengthening. H_2O_2 also diffuses into the cell, leading to a localized peripheral intracellular increase. Localized external H_2O_2 production also increases Ca^{2+} channel activity (3). Downstream events include Ca^{2+} wave propagation during the subsequent 10 to 60 sec (4), followed by Ca^{2+}_{m} increase (5) and mitochondrial ROS production (6). FCCP, carbonylcyanide *p*-trifluoromethoxyphenyl hydrazone.

METHODS

Embryo Culture

Fucus serratus embryos were cultured on glass cover slips fitted to the base of culture dishes in filtered seawater for 24 h in unidirectional light at 16°C, as described previously (Goddard et al., 2000). All experiments were performed using two-celled embryos. Dishes were perfused during experiments on the stage of a Nikon Diaphot 300 inverted microscope (Tokyo, Japan) with a gravity perfusion system that allowed rapid solution changeover.

Cytosolic Ca^{2+} Measurements

Cytosolic Ca^{2+} (Ca^{2+}_{cyt}) was measured in rhizoid cells using Calcium green–dextran (10 kD) ratioed against Texas red–dextran (10 kD; Molecular Probes, Eugene, OR) (Goddard et al., 2000). Dyes were dissolved to a final concentration of 1 mM in an artificial intracellular solution (200 mM KCl, 10 mM Hepes, and 550 mM mannitol, pH 7.0), pressure microinjected (Taylor et al., 1996; Goddard et al., 2000) using pipettes fabricated from 1.2-mm filamented borosilicate glass, and dry beveled (Taylor et al., 1996). In some cells, the Ca^{2+} chelator dibromo glycine, N_1N^1-(1,2-ethanediylbis(oxy-2,1-phenylene)) bis(N-carboxymethyl))-tetrapotassium salt (intracellular concentration of 4 mM) was microinjected along with the Ca^{2+} dyes to buffer Ca^{2+}_{cyt} changes. Ca^{2+} dyes were injected to a final intracellular concentration of 10 to 50 μM. Embryos were incubated in 0.1 to 0.2 M sorbitol to reduce internal turgor pressure during microinjection and recovered in seawater for >1 h before measurements were taken. Images were acquired using a Bio-Rad 1024 confocal microscope (Hemel Hampstead, UK) equipped with a krypton/argon laser. Calcium green and Texas red were excited at 488 nm (523 nm emission) and 567 nm (605 nm emission), respectively. Images were acquired using TIMECOURSE software (Bio-Rad) and ratioed using TIMECOURSE (Bio-Rad) or LUCIDA (Kinetic Imaging, Liverpool, UK) software. Calcium green/Texas red fluorescence ratio (R) values were calibrated from R_{min} and R_{max} (Grynkiewicz et al., 1985). Dye-loaded cells were perfused alternatively with Ca^{2+}-free seawater (containing 0.1 mM EGTA) and 50 mM Ca^{2+}-seawater to obtain R_{min} and R_{max} values, respectively. All calibration solutions contained 100 μM ionomycin (Calbiochem, Nottingham, UK). Ca^{2+}_{cyt} values were calculated using the formula $[Ca^{2+}]_{cyt} = K_d(R - R_{min})/(R_{max} - R)$. The K_d of Calcium green = 190 nM.

Intracellular Reactive Oxygen Species Measurements

Reactive oxygen species (ROS) production was monitored as oxidation of 5- (and 6-) chloromethyl-2′,7′-dichlorodihydrofluorescein diacetate (CM-$DCFH_2$-DA; Molecular Probes). Different dye-loading protocols were used to visualize preferentially either early peripheral cytosolic ROS production or longer term mitochondrial production. For visualization of early ROS increases in both the cytosol and the mitochondria, embryos were incubated in 100 μM CM-$DCFH_2$-DA in 1% ethanol for 20 min. Dye was retained in the experimental solution throughout the experiment. For preferential visualization of mitochondrial ROS production, cells were washed in seawater for 20 min before experiments. This removed dye from the cytosolic, but not the mitochondrial, compartment. Confocal images were obtained after excitation at 488 nm and emission at 522 nm. Because CM-$DCFH_2$-DA is a nonratiometric dye, we checked for any changes in fluorescence caused by a decrease in cell volume during hyperosmotic shock by simultaneously monitoring the fluorescence of microinjected Texas red–dextran (see above).

To estimate intracellular ROS production in nonstressed cells and during hyperosmotic shock, we used an in vivo calibration protocol. First, an in vitro calibration curve of the fluorescence of droplets of CM-$DCFH_2$ (chemically hydrolyzed from CM-$DCFH_2$-DA as indicated by the manufacturer) mixed with known concentrations of H_2O_2 (calibration curve A) was constructed together with an in vitro calibration curve of the fluorescence of droplets of various known concentrations of Texas red (calibration curve B). Rhizoid cells were injected with equal proportions of Texas red–dextran and CM-$DCFH_2$-DA. The average cellular fluorescence of each dye was monitored before and after hyperosmotic shock treatment. The concentration of Texas red, and thus the concentration of DCFH, was determined from calibration curve B. Using calibration curve A, we calculated the intracellular total ROS production that gave rise to the observed fluorescence.

Mitochondrial Localization

Mitochondria were localized after incubation with 0.1 μM MitoTracker Red (Molecular Probes) for 30 min or 0.2 μM MitoTracker Green (Molecular Probes) for 1.5 h. Mitochondrial membrane potential was monitored using the lipophilic cationic probe tetramethylrhodamine ester (TMRE; 0.1 μM for 5 min) (Molecular Probes). Each dye was dissolved in 0.1% DMSO in filtered seawater. To confirm the mitochondrial localization of MitoTracker dyes, embryos labeled with MitoTracker red or MitoTracker green were fixed, embedded, and sectioned for transmission electron microscopy as described previously (Brownlee and Pulsford, 1988) but without osmium after fixation. Confocal fluorescence images of sections mounted on 3- × 1-mm slot grids (0.1 to 0.5 μm) were acquired, and sections were exposed subsequently to osmium vapor from a drop of osmium tetroxide in a closed petri dish. They were then stained in 4% methyl acetate and lead citrate and viewed with a JEOL 200 CX electron microscope. This allowed the direct identification of fluorescent cellular structures.

TMRE enters mitochondria in a membrane potential–dependent manner. Mitochondrial accumulation of TMRE has been shown to cause the quenching of fluorescence, whereas mitochondrial depolarization induces TMRE release from mitochondria and a consequent increase in cellular fluorescence (Zimmermann, 2000). Thus, changes in TMRE fluorescence have been used to monitor mitochondrial membrane potential changes. TMRE fluorescence was monitored with the confocal microscope at 568-nm excitation and 605-nm emission. Cells loaded simultaneously with CM-$DCFH_2$-DA and MitoTracker red or with X-rhod-FF ((Molecular Probes; see below) and MitoTracker green were scanned at 488/568 nm (excitation wavelengths) and 522/605 nm (emission wavelengths).

Inhibitors

The mitochondrial uncoupler carbonylcyanide *p*-trifluoromethoxyphenyl hydrazone (Sigma, Poole, UK) was dissolved in 0.1% DMSO and filtered seawater (final concentration of 1 μM). The NADPH oxidase inhibitor diphenyleneiodonium (Sigma) was dissolved in 0.1% DMSO to a final concentration of 10 μM in filtered seawater. Cells were exposed to inhibitors for 1 h before the beginning of the experiment, and inhibitors also were included in the perfusing solutions.

The phospholipase C inhibitor U73122 or its inactive analog U73343 was dissolved in 0.1% DMSO and filtered seawater (final concentration of 10.0 μM), and cells were preincubated for 2 h. Catalase (Sigma) was used at a concentration of 450 μg/mL.

Mitochondrial Ca^{2+}

X-rhod-FF was used to monitor mitochondrial Ca^{2+} changes. X-rhod-FF has a net positive charge, which facilitates its sequestration inside mitochondria by potential-driven uptake. Cells were loaded with 2 μM X-rhod-FF AM (0.1% DMSO) for 1.5 h. The residual extracellular and cytosolic dye was eliminated by washing in seawater for 2 h. The mitochondrial localization of the dye was checked by coloading the cells with MitoTracker green. Confocal images of X-rhod-FF fluorescence were obtained at 568 nm (excitation) and 605 nm (emission).

Inositol 1,4,5-Triphosphate Photorelease

Rhizoid cells were microinjected with a mixture of caged inositol 1,4,5-triphosphate [Ins(1,4,5)P_3] (Calbiochem; final intracellular concentration of 10 μM) and Calcium green–dextran and Texas red–dextran as described above. To monitor ROS production, cells were injected with Ins(1,4,5)P_3 and Texas red–dextran (final intracellular concentration of 10 to 50 μM) and then incubated with CM-$DCFH_2$-DA as described above. Photorelease was achieved with a UV light–pulsed nitrogen laser (10-ns pulses, 20 Hz for 1 s) (VSL337; Laser Science, Cambridge, MA) delivered via the microscope objective and focused to an adjustable spot via a beam expander and adjustable focusing lens (Goddard et al., 2000). Laser intensity was adjusted with a diaphragm in the delivery optics to a level that caused the photorelease of Ins(1,4,5)P_3 but did not by itself induce an oxidative burst. Control cells were microinjected only with Texas red–dextran, loaded with CM-$DCFH_2$-DA, and exposed to identical laser excitation.

Patch Clamping

Spheroplasts were obtained from the apices of Fucus rhizoid cells using laser microsurgery of the cell wall, as described previously (Taylor and Brownlee, 1992; Taylor et al., 1996). Cell-attached recordings were made from apical protoplasts using conventional patch-clamp techniques (Taylor et al., 1996). The reference electrode consisted of an Ag/AgCl pellet in a holder containing seawater and was connected to the bath via a 3% agar bridge. Patch pipettes were fabricated from borosilicate glass (GC150TF; Clark, Pangbourne, UK) with a Narishige pipette puller (P-833; Narishige, Tokyo, Japan). Electrodes were dipped briefly in 0.001% polylysine solution (Sigma) before back filling with ultrafiltered pipette solution (30 mM $CaCl_2$, 30 mM KCl, and 10 mM Hepes, pH 7.8). Patch-clamp recordings were obtained with an Axopatch 1D amplifier (Axon Instruments, Foster City, CA), filtered at 5 kHz, and analyzed with PCLAMP software (Axon Instruments).

Upon request, all novel materials described in this article will be made available in a timely manner for noncommercial research purposes. No restrictions or conditions will be placed on the use of any materials described in this article that would limit their use for noncommercial research purposes.

ACKNOWLEDGMENTS

Supported by Fundação para a Ciência e Tecnologia, Portugal (S.M.C.), and the Biotechnology and Biological Science Research Council and the Natural Environment Research Council, United Kingdom (C.B. and A.R.T.).

Received March 22, 2002; accepted June 26, 2002.

REFERENCES

Allan, A., and Fluhr, R. (1997). Two distinct sources of elicited reactive oxygen species in tobacco epidermal cells. Plant Cell **9,** 1559–1572.

Bac, Y.S., Kang, S.W., Seo, M.S., Baines, I.C., Teckle, E., Chock, P.B., and Rhee, S.G. (1997). Epidermal growth factor (EGF)-induced generation of hydrogen peroxide. J. Biol. Chem. **272,** 217–221.

Berger, F., and Brownlee, C. (1995). Physiology and development of protoplasts obtained from *Fucus* embryos using laser microsurgery. Protoplasma **186,** 63–71.

Bowie, A., and O'Neill, L.A. (2000). Oxidative stress and nuclear factor-kappaB activation: A reassessment of the evidence in the light of recent discoveries. Biochem. Pharmacol. **59,** 13–23.

Bradley, D., Kjellbom, P., and Lamb, C. (1992). Elicitor- and wound-induced oxidative cross-linking of a proline-rich plant cell wall protein: A novel, rapid defense response. Cell **70,** 21–30.

Brownlee, C., and Pulsford, A. (1988). Visualization of the cytoplasmic Ca^{2+} gradient in *Fucus serratus* rhizoids: Correlation with cell structure and polarity. J. Cell Sci. **91,** 249–256.

Brownlee, C., and Wood, J.W. (1986). A gradient of cytosolic free calcium in growing rhizoid cells of *Fucus serratus*. Nature **320,** 624–626.

Desikan, R., Hancock, J.T., Coffey, M.J., and Neill, S.J. (1996). Generation of active oxygen in elicited cells of *Arabidopsis thaliana* is mediated by a NADPH oxidase-like enzyme. FEBS Lett. **382,** 213–217.

Desikan, R., Neill, S.J., and Hancock, J.T. (2000). Hydrogen peroxide-induced gene expression in *Arabidopsis thaliana*. Free Radical Biol. Med. **28,** 773–778.

Duchen, M.R. (2000). Mitochondria and calcium: From cell signaling to cell death. J. Physiol. **529,** 57–68.

Finkel, T. (1998). Oxygen radicals and signaling. Curr. Opin. Cell Biol. **10,** 248–253.

Frahry, G., and Schopfer, P. (1998). Inhibition of O_2^- reducing activity of horseradish peroxidase by diphenyleneiodonium. Phytochemistry **48,** 223–227.

Fry, S.C., Willis, S.C., and Patterson, A.E. (2000). Evidence for covalent linkage between xyloglucan and acidic pectins in suspension-cultured rose tissue. Planta **211,** 275–286.

Goddard, H., Manison, N., Tomos, D., and Brownlee, C. (2000). Elemental propagation of calcium signals in response-specific patterns determined by environmental stimulus strength. Proc. Natl. Acad. Sci. USA **97,** 1932–1937.

Grant, J., and Loake, G. (2000). Role of reactive oxygen intermediates and cognate redox signaling in disease resistance. Plant Physiol. **124,** 21–29.

Grijalba, M.T., Vercesi, A.E., and Schreier, S. (1999). Ca^{2+}-induced increased lipid packing and domain formation in submitochondrial particles: A possible early step in the mechanism of Ca^{2+}-stimulated generation of reactive oxygen species by the respiratory chain. Biochemistry **38,** 13279–13287.

Grynkiewicz, G., Poenie, M., and Tsien, R.Y. (1985). A new generation of Ca^{2+} indicators with greatly improved fluorescence properties. J. Biol. Chem. **260,** 3440–3450.

Guan, L.M., Zhao, J., and Scandalios, J.G. (2000). *Cis*-elements and *trans*-factors that regulate expression of the maize *Cat1* antioxidant gene expression in response to ABA and osmotic stress: H_2O_2 is the likely intermediary signaling molecule for the response. Plant J. **22,** 87–95.

Hoth, M., Fanger, C., and Lewis, R. (1997). Mitochondrial regulation of store-operated calcium signaling in T lymphocytes. J. Cell Biol. **137,** 633–648.

Levine, A., Tenhaken, R., Dixon, R., and Lamb, C. (1994). H_2O_2 from the oxidative burst orchestrates the plant hypersensitive disease resistance response. Cell **79,** 583–593.

Maxwell, D., Wang, Y., and McIntosh, L. (1999). The alternative oxidase lowers mitochondrial reactive oxygen production in plant cells. Proc. Natl. Acad. Sci. USA **96,** 8271–8276.

Minibayeva, F., Kolesnikov, O., and Gordon, L. (1998). Contribution of plasma membrane redox system to the superoxide production by wheat root cells. Protoplasma **205,** 101–106.

Morel, Y., and Barouki, R. (1999). Repression of gene expression by oxidative stress. Biochem. J. **342,** 481–496.

Park, M.K., Ashby, M.C., Erdemli, G., Petersen, O.H., and Tepikin, A.V. (2001). Perinuclear, perigranular and sub-plasmalemmal mitochondria have distinct functions in the regulation of cellular calcium transport. EMBO J. **20**, 1863–1874.

Pastori, Y., and del Rio, L.A. (1997). Natural senescence of pea leaves: An activated oxygen-mediated function for peroxisomes. Plant Physiol. **113,** 411–418.

Pei, Z.-M., Murata, Y., Benning, G., Thomine, S., Klusener, B., Allen, G., Grill, E., and Schroeder, J.I. (2000). Calcium channels activated by hydrogen peroxide mediate abscisic acid signalling in guard cells. Nature **406,** 731–734.

Pu, R., and Robinson, K.R. (1998). Cytoplasmic calcium gradients and calmodulin in the early development of the fucoid alga *Pelvetia compressa*. J. Cell Sci. **111,** 3197–3207.

Pugin, A., Frachisse, J.-M., Tavernier, E., Bligny, R., Gout, E., Douce, R., and Guern, J. (1997). Early events induced by the elicitor cryptogein in tobacco cells: Involvement of a plasma membrane NADPH oxidase and activation of glycolysis and the pentose phosphate pathway. Plant Cell **9,** 2077–2091.

Reichheld, J.-P., Vernoux, T., Lardon, F., Van Montagu, M., and Inzé, D. (1999). Specific checkpoints regulate plant cell cycle progression in response to oxidative stress. Plant J. **17,** 647–656.

Rizzuto, R., Bernardi, P., and Pozzan, T. (2000). Mitochondria as all-round players of the calcium game. J. Physiol. **529,** 37–47.

Shackelford, R.E., Kaufmann, W.K., and Paules, R.S. (2000). Oxidative stress and cell cycle checkpoint function. Free Radical Biol. Med. **28,** 1387–1404.

Subbaiah, C.C., et al. (1998). Mitochondrial contribution to the anoxic Ca^{2+} signal in maize suspension-cultured cells. Plant Physiol. **118,** 759–771.

Tan, S., Sagara, Y., Liu, Y., Maher, P., and Schubert, D. (1998). The regulation of reactive oxygen species production during programmed cell death. J. Cell Biol. **141,** 1423–1432.

Taylor, A., and Brownlee, C. (1992). Localized patch clamping of plasma membrane of a polarized plant cell. Plant Physiol. **99,** 1686–1688.

Taylor, A.R., Manison, N., Fernandez, C., Wood, J., and Brownlee, C. (1996). Spatial organization of calcium signaling involved in cell volume control in the *Fucus* rhizoid. Plant Cell **8,** 2015–2031.

Zhu, H., Bannenberg, G.L., Moldéus, G.L., and Shertzer, H.G. (1994). Oxidation pathways for the intracellular probe 2′,7′-dichlorofluorescein. Acta Toxicol. **68,** 582–587.

Zimmermann, B. (2000). Control of Ins(1,4,5)P_3-induced Ca^{2+} oscillations in permeabilized blowfly salivary gland cells: Contribution of mitochondria. J. Physiol. **525,** 707–719.